The Astrophysical Journal Letters, 891:L32 (7pp), 2020 March 10 https://doi.org/10.3847/2041-8213/ab77c8

The Influence of Late-stage Nuclear Burning on Red Supergiant Supernova Light Curves

Viktoriya Morozova[1], Anthony L. Piro[2], Jim Fuller[3], and Schuyler D. Van Dyk[4]
[1] Department of Physics, The Pennsylvania State University, University Park, PA 16802-6300, USA; vzg5138@psu.edu
[2] The Observatories of the Carnegie Institution for Science, 813 Santa Barbara Street, Pasadena, CA 91101, USA
[3] TAPIR, Walter Burke Institute for Theoretical Physics, Mailcode 350-17, Caltech, Pasadena, CA 91125, USA
[4] Caltech/Spitzer Science Center, Caltech/IPAC, Mailcode 100-22, Pasadena, CA 91125, USA
Received 2019 December 20; revised 2020 February 16; accepted 2020 February 19; published 2020 March 9

Abstract

Many Type II supernovae (SNe) show hot early (∼30 days) emission, and a diversity in their light curves extending from the Type IIP to the Type IIL, which can be explained by interaction with dense and confined circumstellar material (CSM). We perform hydrodynamical simulations of red supergiants to model the ejection of CSM caused by wave heating during late-stage nuclear burning. Even a small amount of deposited energy (10^{46}–10^{47} erg), which is roughly that expected due to waves excited by convection in the core, is sufficient to change the shapes of SN light curves and bring them into better agreement with observations. As a test case, we consider the specific example of supernova (SN) 2017eaw, which shows that a nuclear burning episode is able to explain the light curve if it occurs ∼150–450 days prior to core collapse. Due to the long timescale that it takes for the low-energy shock to traverse the star, this would manifest as a pre-SN outburst ∼50–350 days prior to the full-fledged SN. Applying work like this to other SNe will provide a direct connection between the SN and pre-SN outburst properties, which can be tested by future wide field surveys. In addition, we show that our models can qualitatively explain the short-lived "flash-ionization" lines seen in the early spectra of many Type II SNe.

Unified Astronomy Thesaurus concepts: Hydrodynamics (1963); Supernovae (1668); Type II supernovae (1731); Core-collapse supernovae (304); Radiative transfer (1335)

1. Introduction

The pre-explosion images of hydrogen-rich, plateau-type supernovae (SNe IIP) unambiguously identify red supergiants (RSGs) as their progenitors (Smartt 2009; Van Dyk 2017). Yet numerical models of SN IIP light curves performed with up-to-date RSG models from stellar evolution codes still cannot reproduce some of the basic observed features, such as fast rise and early maxima of the light curves and the bright emission over the first ∼10–30 days (Moriya et al. 2017, 2018; Morozova et al. 2017, 2018; Paxton et al. 2018). These studies show that addition of a dense circumstellar material (CSM) on top of the RSG models can help to bring them in a better agreement with the observations and may explain the full diversity from Type IIP (plateau) to IIL (linear) subclasses. From the physical point of view, this may be attributed to the fact that the CSM introduces a distinctly shorter diffusion timescale into the model (a few tens of days, compared to a ∼100 days timescale of the bulk of the RSG envelope), while the larger radius leads to less adiabatic cooling and brighter emission. However, the underlying origin of the dense CSM remains a mystery. Models in which the CSM is produced by a dense wind require mass-loss rates of at least $10^{-3}\,M_{\odot}\,\mathrm{yr}^{-1}$, and it is not clear if such high rates are physically plausible.

A possible answer to this question is the ejection of matter by a RSG at the late stages of its evolution. The energy required for the ejection can be produced by vigorous late-stage core nuclear burning processes, and deposited into the envelope by means of wave transport (Quataert & Shiode 2012; Shiode & Quataert 2014; Quataert et al. 2016; Fuller 2017). This scenario implies that the luminosity of the progenitor star should change in the years prior to the supernova (SN) explosion, either in a steady manner or in the form of an outburst.

To date, there has been no unambiguous detection of an outburst preceding a regular SN IIP or IIL (here, we do not discuss Type IIn SNe, for which pre-explosion outbursts have been detected; see Ofek et al. 2013, 2014). Studies of the available pre-explosion images (Kochanek et al. 2017; Johnson et al. 2018; O'Neill et al. 2019) report no significant variability of the SN IIP progenitors in the last several years of their lives. At the same time, these images are often sparsely sampled and rarely cover the infrared bands, which contain the largest fraction of the RSG emission. Interpretation of the pre-explosion data is challenged by the fact that we do not yet have a clear idea about the strength, time, and duration of the pre-explosion outbursts that would be sufficient to explain the observed SN IIP light curves.

In this Letter, we attempt to clarify these questions by drawing a more consistent picture of the influence of pre-explosion wave energy transport on SN light curves. Using numerical simulations, we model the hydrodynamics of the matter ejection caused by wave energy transport in a parameterized way. We vary the amount of energy deposition in the stellar envelope, and the time between envelope heating and the core-collapse explosion. This way, we generate a progression of light curves that would correspond to consequent snapshots of the progenitor profile after the outburst, showing that the pre-explosion ejection of matter changes the SN light curves in a way that improves their agreement with the observations. Using an example of a well-observed typical IIP SN 2017eaw, we deduce the most likely values of the outburst energy and time between the outburst and the core collapse, finding that they are similar to expectations of wave heating models.

In Section 2, we describe our numerical setup. Section 3 contains our main results, while Section 4 is devoted to the conclusions and discussion.

2. Numerical Setup

We perform our study using the publicly available code SNEC (Morozova et al. 2015). The code solves Lagrangian hydrodynamics coupled with radiation transport in the flux-limited diffusion approximation. This approximation is well suited for obtaining the bolometric light curves of SNe II starting from 1 to 2 days after the shock breakout and until the end of the plateau phase. We work with a solar metallicity, $15\,M_\odot$ (at zero-age main sequence (ZAMS)) stellar evolution model from the KEPLER set by Sukhbold et al. (2016), evolved to the pre-collapse RSG stage. This model is in agreement with the bolometric luminosity $(1.2 \pm 0.2) \times 10^5\,L_\odot$ deduced from the pre-explosion images of SN 2017eaw by Van Dyk et al. (2019).[5] The final mass of the RSG at the onset of core collapse is $12.6\,M_\odot$, while its radius is $841\,R_\odot$.

In the first stage of our simulations, we model the deposition of energy by convectively excited waves during a vigorous late-stage nuclear burning episode into the RSG envelope (it could be core Ne or O burning), as outlined by Fuller (2017). However, instead of modeling the wave transport between the core and the envelope self-consistently, we parameterize our setup in terms of the energy injected at the base of the hydrogen envelope. To deposit the energy into the model, we first excise a large part of its core, down to the density values of $\sim 1\,\mathrm{g\,cm^{-3}}$ ($4.31\,M_\odot$ in terms of the excised inner mass). This enables us to simulate a very weak energy deposition with a reasonably large numerical time step, while still keeping the inner boundary well inside the stellar core. In the current version of SNEC, the velocity at the inner boundary is always taken to be zero. We employ a commonly used thermal bomb mechanism, but instead of putting the energy into the innermost grid points, we inject it all in a single grid point at the density of $\sim 7 \times 10^{-6}\,\mathrm{g\,cm^{-3}}$. The duration of the thermal bomb is chosen so that the heating rate is equal to $10^7\,L_\odot$, as in Figure 4 of Fuller (2017). We vary the injected energy, $E_{\rm inj}$, within the range of values expected in a standard RSG (see Figure 5 of Fuller 2017), namely, between 1×10^{46} erg and 2×10^{47} erg, in steps of 0.5×10^{46} erg. For reference, the binding energy of all material above the thermal bomb in this model is 7.7×10^{47} erg.

The deposition of energy initiates a weak shock wave propagating through the envelope of the RSG. Once this shock wave reaches the surface of the star, some part of the envelope material gets ejected and the model starts expanding. Depending on the value of $E_{\rm inj}$, not all of the material ejected by the weak shock wave becomes unbound, and part of it may later fall back onto the star. We follow the evolution of the model for ≈900 days and collect the density, temperature, and velocity profiles at different times after the energy injection, $t_{\rm inj}$.

In the second stage of our simulations, we explode these profiles in SNEC, this time using our regular core-collapse SN setup (Morozova et al. 2015, 2018). As a result, we obtain a two-dimensional grid of SN light curves corresponding to different energies $E_{\rm inj}$ and times $t_{\rm inj}$ between the energy injection and the core collapse.

Since this study uses as an example a well-observed SN 2017eaw, we restrict ourselves to a single value of ^{56}Ni mass, $M_{\rm Ni} = 0.075\,M_\odot$, which was found to fit the radioactive tail of this SN in Van Dyk et al. (2019).[6] In our models, we mix radioactive ^{56}Ni up to $5\,M_\odot$ in mass coordinate. In addition, we use a single value of the explosion energy (parameter $E_{\rm fin}$ in SNEC), which fits the plateau part of SN 2017eaw, 0.75×10^{51} erg. The thermal bomb energy in SNEC is computed as $E_{\rm bomb} = E_{\rm fin} - E_{\rm init}$, where $E_{\rm init}$ is the initial energy of the model. Before exploding the models, we reattach their C/O cores back, assuming that they have not been affected by the weak energy injection. Then, we excise the inner $1.6\,M_\odot$ of material that forms a neutron star, and deposit the thermal bomb energy into the first few grid points with the total mass of $\Delta M = 0.02\,M_\odot$ for a duration of 1 s.[7] We compare the resulting light curves to the data of SN 2017eaw and find the best-fitting model by minimizing χ^2.

The main limitation of our study comes from the fact that SNEC does not have a nuclear burning routine and a prescription for the convective energy transport, which are essential for supporting the stellar structure in the evolutionary codes. It does not cause any problems in quick and energetic SN explosions, which SNEC was originally designed to simulate. However, following a stellar evolution model without these physical components for several hundreds of days between the pre-SN outburst and the core collapse causes distortions in the outer layers of the model. This leads to artificial bumps and irregularities in the pre-explosion velocity and density profiles (like in the bottom panel of Figure 1, and in Figure 2), which are otherwise expected to be smoother.[8] Nevertheless, we argue that SNEC is able to capture the hydrodynamics of the outburst, the near-surface density profile, and to give a robust qualitative prediction of its influence on the final SN light curves. The aim of this work is to draw the connection between the late-stage nuclear burning and the shape of the SN IIP light curves, as well as to get a general idea of the energetics and timing of the pre-explosion outbursts. In the future, we plan to perform a more extended study of the outbursts with an improved setup.

3. Results

3.1. Effect on Pre-SN Structure

Figures 1 and 2 illustrate the evolution of the RSG profile in the first few hundreds of days after the energy has been injected at the base of its hydrogen envelope ($E_{\rm inj} = 5.0 \times 10^{46}$ erg in both figures). The top panel of Figure 1 shows the original pre-explosion density profile of the KEPLER model. The bottom panel of Figure 1 shows the velocity and temperature profiles of this model at different moments of time after the energy injection. Note that the time it takes for a weak shock wave to propagate through the hydrogen envelope all the way to the surface is ∼100 days in this model, a significant fraction of the time between energy injection and core collapse.

The velocity evolution in the bottom panel of Figure 1 reflects the pre-explosion density structure of the progenitor

[5] Van Dyk et al. (2019) used Geneva evolutionary tracks (Georgy et al. 2013) to estimate the ZAMS mass of the progenitor as $\approx 15\,M_\odot$, but we arrive to the same conclusion based on the pre-explosion luminosities of KEPLER models.

[6] Buta & Keel (2019) obtained a higher ^{56}Ni mass of $0.115\,M_\odot$ for the same SN.

[7] After re-attaching the cores, we do not attempt to smooth the density profiles at the core-envelope interface. This leads to artificial bumps at the transition between plateau and radioactive tails in the final SN light curves (see Figure 4). In reality, Rayleigh–Taylor instabilities occurring when the shock wave propagates through the sharp density gradients will smooth the profiles and, consequently, the light curves (see, for example, Paxton et al. 2018). However, this effect is not important for the conclusions of the present study, and we leave it for future work.

[8] In fact, these bumps may in part be real and attributed to the wave heating. However, in our current setup it is not possible to separate the real physical effect from the numerical artifacts.

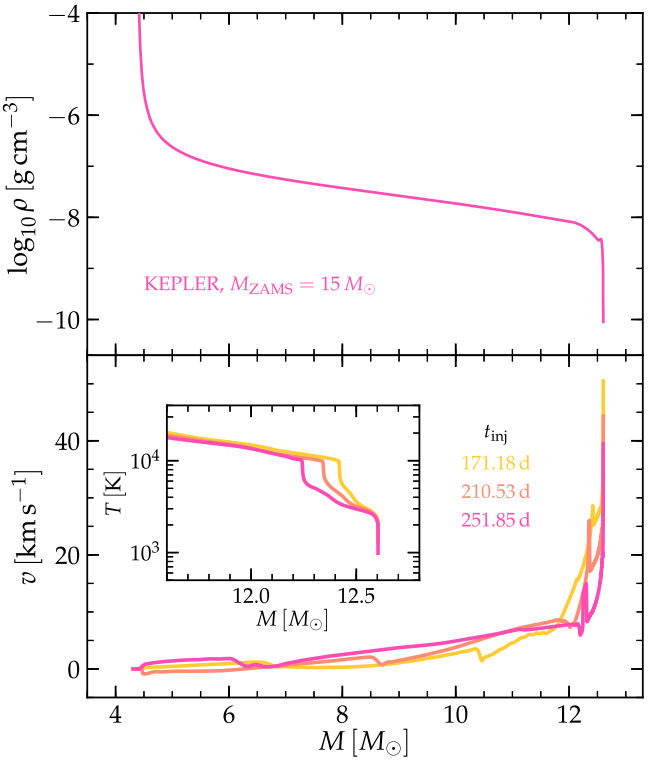

Figure 1. Top panel: RSG density profile used in our study. We mimic the energy input from the late-stage core nuclear burning by injecting the chosen amount of energy, $E_{\rm inj}$, at the base of the hydrogen envelope (in the model shown here, we inject 5×10^{46} erg of energy at the point where the density is $\approx 7 \times 10^{-6}$ g cm^{-3}). Bottom panel: velocity profiles at the different times after the energy injection. The inset shows the corresponding temperature profiles in the outer regions of the envelope.

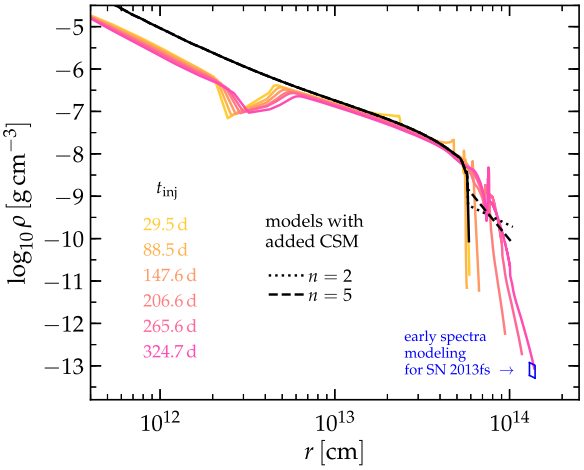

Figure 2. Evolution of the density profile of the RSG during the first few hundreds of days after the energy has been injected at the base of its hydrogen envelope. The injected energy is $E_{\rm inj} = 5 \times 10^{46}$ erg. The black solid curve shows the model before the energy injection. The low-density regions at the radial coordinate $\sim 3 \times 10^{12}$ cm roughly correspond to the energy injection regions, while the irregularities at $\sim 8 \times 10^{13}$ cm are due to the distortion of the stellar evolution progenitors in SNEC (see the last paragraph of Section 2). The black dashed and dotted lines illustrate artificial CSM, which was shown to improve agreement between the simulated and the observed SN II light curves in Morozova et al. (2017, 2018) and Morozova & Stone (2018). The blue rectangle shows the CSM parameters deduced from the modeling of early spectra of SN 2013fs by Yaron et al. (2017).

RSG. The RSG model has a shallower density profile in the bulk of its envelope, which transitions into a steeper profile at about $0.5\,M_\odot$ below the surface (top panel of Figure 1). As a consequence, the velocity gained by the outermost $\sim 0.5\,M_\odot$ of the envelope after the passage of the weak shock wave launched by energy injection is noticeably higher than the velocity of the inner envelope regions. After the initial expansion, part of this outer material decelerates and at later times starts falling back toward the star.

The inset in the bottom panel of Figure 1 illustrates the temperature evolution in this model. The expansion of the ejected material quickly cools it down to temperatures below $\sim$6000 K. At this temperature, the hydrogen and helium recombine, which leads to a dramatic drop in the opacity of the stellar material. Therefore, by day $\sim$250 the outermost 0.4–0.5 $M_\odot$ of the model from Figure 1 are effectively transparent to the optical emission. This is consistent with Figure 11 of Fuller (2017), where the pre-heated models have up to a few tenths of a solar mass of material above the photosphere after the outburst. At the same time, this material does not have enough time to cool down to temperatures below $\sim$1000 K, at which it would start to form dust and obscure the progenitor. In the model shown in Figure 1, only the last few grid points reach the temperatures below 10^3 K. These cells contain the amount of mass of the order of $10^{-4}\,M_\odot$, and they are likely affected by the boundary conditions used in SNEC. Similarly, the material expelled due to wave heating in MESA models by Fuller (2017) does not cool down to temperatures below 2000 K prior to core collapse. For this reason, we do not expect a significant dust formation in the first few hundreds of days after nuclear burning episode causing the wave heating, unless the ejected material can cool down further through the mechanisms that are not taken into account in both codes (e.g., cooling by lines).

In Figure 2, we show the density profiles of the same model as a function of radial coordinate, at different moments of time after the energy injection. Before day $\sim$100, a weak shock wave can be seen propagating through the envelope. After it reaches the surface, the outermost layers of the model start to expand. The black solid curve shows the original RSG profile before the energy injection. For comparison, the black dashed and dotted lines show the models of artificially added CSM with density profile $\rho \propto r^{-n}$, where $n = 2$ corresponds to the case of a steady stellar wind. The mass of the added CSM is $0.6\,M_\odot$ in both models. In our earlier works (Morozova et al. 2017, 2018; Morozova & Stone 2018) we employed these CSM models to get a better agreement between the simulated and the observed SN II light curves at early times (first $\sim$30 days). We suggest that the wave heating may serve as a theoretically justified mechanism for the formation of such CSM. In addition, the blue rectangle shows the CSM parameters confined by the analysis of early spectra of SN 2013fs in Yaron et al. (2017).[9]

[9] Yaron et al. (2017) used a steady wind prescription for the CSM, namely, $\rho = \dot{M}/(4\pi v_{\rm wind} r^2)$, where $v_{\rm wind}$ is the wind velocity and $\dot{M}$ is the mass loss in solar masses per year. The blue rectangle shown in Figure 2 corresponds to $v_{\rm wind} = 100$ km s^{-1}, $\dot{M} = (2\text{–}4) \times 10^{-3}\,M_\odot$ yr^{-1}, and the emitting radius $(1.3\text{–}1.4) \times 10^{14}$ cm. At the same time, their analysis does not probe the density of material below the emitting radius, and we see no reason to interpolate the constant $\dot{M} = 3 \times 10^{-3}\,M_\odot$ yr^{-1} wind profile all the way down to the RSG surface. Indeed, our models suggest that the CSM may become much denser in the immediate vicinity of the RSG, without contradicting to Yaron et al. (2017).

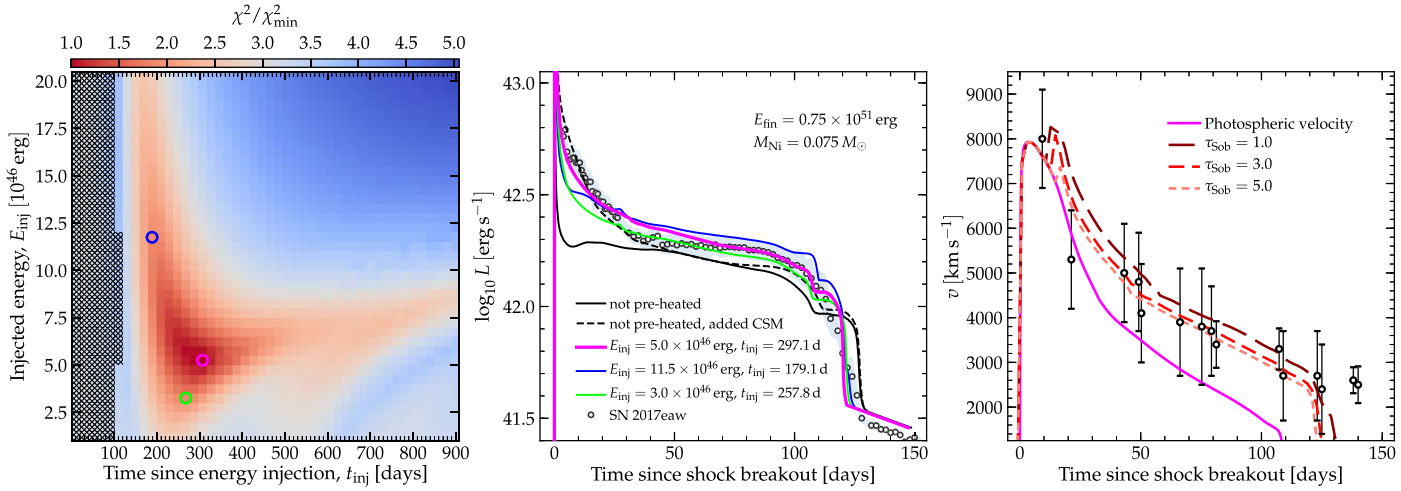

Figure 3. Left panel: color-coded distribution of $\chi^2/\chi^2_{\rm min}$ across the $E_{\rm inj}$-$t_{\rm inj}$ parameter space for the KEPLER 15 $M_\odot$ model. The gray shaded region covers the times during which the weak shock wave launched by energy injection propagates between the base of the hydrogen envelope and the stellar surface (in those times, no visible outburst is expected from the progenitor). The χ^2 itself is determined by the comparison of the SN light curves obtained from these models to the bolometric light curve of SN 2017eaw. All SN explosions are performed with the same set of parameters, $E_{\rm fin} = 0.75 \times 10^{51}$ erg and $M_{\rm Ni} = 0.075\,M_\odot$. The magenta circle corresponds to the minimum χ^2, while the lime and blue circles provide examples of reasonably well-fitting models with smaller and larger $E_{\rm inj}$, respectively. Middle panel: the bolometric SN light curves of the models from the left panel, compared to the data of SN 2017eaw from Van Dyk et al. (2019). The black solid line shows the light curve obtained from the bare RSG profile with no energy injected at the base of its hydrogen envelope. Right panel: the photospheric velocity of the best-fitting model ($E_{\rm inj} = 5 \times 10^{46}$ erg, $t_{\rm inj} = 297.1$ days), as well as the velocity at the locations $\tau_{\rm Sob} = 1.0$, 3.0 and 5.0 in this model. The black markers show the velocity measured from the Fe II λ5169 lines of SN 2017eaw.

3.2. Effect on SN Light Curve

With envelope density profiles as a function of time, we then model the SN light curves as a function of $E_{\rm inj}$ and $t_{\rm inj}$. We compare the obtained SN light curves to the bolometric light curve of SN 2017eaw and look for the best-fitting parameters by minimizing the χ^2.

The left panel of Figure 3 shows $\chi^2/\chi^2_{\rm min}$ as a function of $E_{\rm inj}$ and $t_{\rm inj}$ in our model. The gray shaded region on the left-hand side of the panel corresponds to the times when the weak shock wave launched by the energy injection has not yet reached the stellar surface. During this time, no observable outburst is expected from the progenitor, and the density profile/SN light curve are not strongly altered. The minimum χ^2 (marked by the magenta circle) corresponds to 5×10^{46} erg of energy being injected ≈297 days before the core collapse. In this model, a visible outburst would take place ≈197 days before the SN. For comparison, the blue and lime circles mark some of the models in which the outburst happens at ≈80 days and ≈160 before the SN, respectively.

The bolometric light curves of these models are shown in the middle panel of Figure 3 with corresponding colors. The black solid line plots the light curve obtained from the original KEPLER 15 $M_\odot$ model without the energy injection, using the same set of SN parameters. Compared to the black solid curve, all models with injected energy show the excess of luminosity, especially in the first ∼40 days of the light curves. The magenta light curve demonstrates the best agreement with the data of SN 2017eaw. For comparison, the dashed black line shows the light curve of the model with artificially added $n = 5$ CSM from Figure 2 (the $n = 2$ model produces almost indistinguishable light curve).

For completeness, in the right panel of Figure 3 we show the velocity measured from the Fe II λ5169 lines of SN 2017eaw. The solid magenta line gives the photospheric velocity of the minimum χ^2 model, and one can see that this velocity significantly underestimates the observed one. However, Paxton et al. (2018) resolved this issue by finding the velocity at the location where the Sobolev optical depth, $\tau_{\rm Sob}$, of the Fe II λ5169 line is ∼1. Indeed, the value of $\tau_{\rm Sob}$ at the photosphere location is much larger than 1 and reaches up to a few hundreds in our models. The three dashed lines in the right panel of Figure 3 show the velocities at the locations where $\tau_{\rm Sob} = 1.0$, 3.0 and 5.0.[10] These velocities are in better agreement with the observations and able to reproduce most of the measurements, except the ones at days ∼20 and ∼140. At the same time, we note that pre-heating itself does not influence the velocities significantly. The difference between the velocities of the minimum χ^2 model and the ones of the bare RSG model is very small, and we do not show the latter in Figure 3 to avoid cluttering the plot.

Figure 4 represents an overview of the SN light curves obtained for the different values of $E_{\rm inj}$ and time $t_{\rm inj}$. It is remarkable that even as little as 1.0×10^{46} erg of energy deposited into the envelope about a year before the core collapse may have a significant impact on the final SN light curve. Therefore, if we want to reproduce the SN IIP light curves with stellar evolution models, we cannot ignore the impact of the late-stage nuclear burning on the progenitor structure. Ideally, the energy deposition should be modeled self-consistently during stellar evolution calculations (as was done, for example, by Fuller 2017), which we hope to address in future works.

Finally, we would like to emphasize the potential of our models to explain one more aspect of the early emission from SNe IIP, namely, so called "flash-ionization" lines. These narrow emission lines appear in the very early spectra of some SNe, and they are generally interpreted as a sign of the shock wave interacting with the CSM (Khazov et al. 2016). These lines are generally short lived and disappear from the spectra

[10] To compute those, we use a table of the fraction of iron atoms in the lower level of transition relevant for the Fe II λ5169 line, which is available in the public version of MESA and credited to Dan Kasen (Paxton et al. 2018).

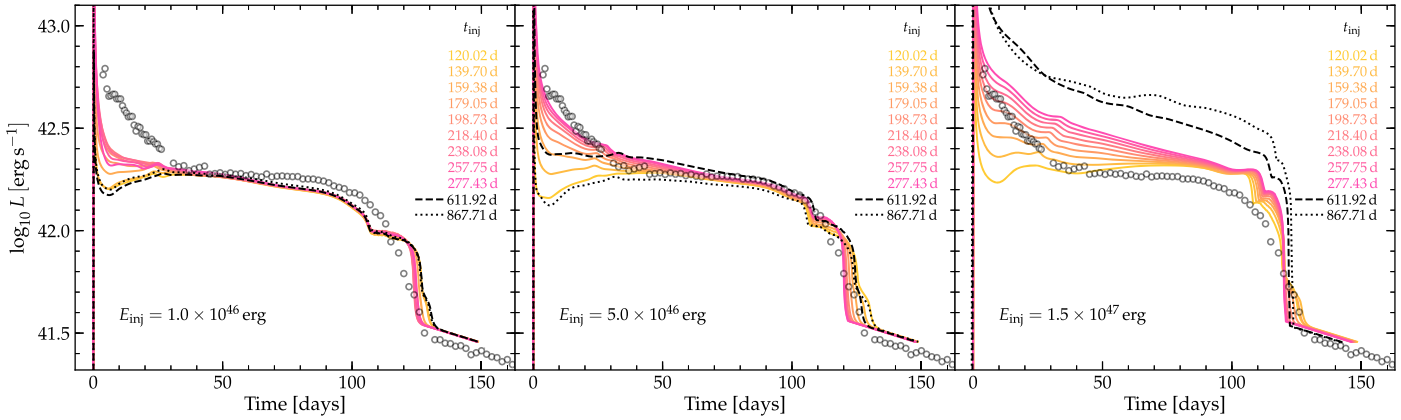

Figure 4. SN light curves of the KEPLER $M_{\rm ZAMS} = 15\,M_\odot$ model, obtained for the different values of $E_{\rm inj}$ and $t_{\rm inj}$. The gray markers show the data of SN 2017eaw. In the models with low $E_{\rm inj}$ (left and middle panels), the density profile keeps expanding until day ∼300 after the energy injection, and the SN light curves obtained from these models show progressive rise in the early bolometric luminosity. After day ∼300, the ejected material decelerates and starts falling back onto the progenitor, reversing the progression of the SN light curves toward their initial state. To avoid clutter in the plots, we show the continuous evolution of the SN light curves until $t_{\rm inj} \approx 300$ days, while plotting the light curves for $t_{\rm inj} \approx 600$ days and $t_{\rm inj} \approx 850$ days in a different style. For the high values of $E_{\rm inj}$, this reversal in the SN light curve progression happens at much later times.

within just a few tens of hours (Yaron et al. 2017). SN 2017eaw also showed a weak narrow H_α emission line in the spectrum taken at ∼1.4 days after the explosion, which did not appear in the subsequent spectrum taken at ∼3.4 days post-explosion (Rui et al. 2019). In a recent study, Dessart et al. (2017) has shown that a cocoon of material of only $\sim 0.01\,M_\odot$ distributed out to about 5–10 stellar radii is sufficient to reproduce the narrow lines seen in the early spectra of SNe 2013cu (Gal-Yam et al. 2014) and 2013fs (Yaron et al. 2017). Recently, Kochanek (2019) suggested an alternative solution, explaining the flash spectroscopy by a collision interface formed between the regular stellar winds in a binary system.

In SNEC, we can pinpoint the moment of shock breakout from our models based on the condition $\tau \approx c/v$, where τ is the optical depth of the material above the shock, v is the shock velocity, and c is the speed of light. The top panel of Figure 5 shows the mass of the material that lays above the shock at the moment of breakout, denoted as $M_{\rm flash}$, as a function of $t_{\rm inj}$ for different $E_{\rm inj}$. The data plotted in Figure 5 appear noisy due to technical issues of determining the position and velocity of the shock wave, but the general trend can be seen very well. For small $t_{\rm inj} < 100$ days, the shock breaks out at the very surface of the models, illuminating only few $10^{-3}\,M_\odot$ of the downstream material. Instead, at $t_{\rm inj} > 100$ days, at which the weak shock wave from the energy injection could substantially preheat and expand the outer layers of the envelope, the subsequent post-explosion shock wave breaks out deeper in mass coordinate and illuminates more material, up to few $10^{-2}\,M_\odot$. The bottom panel of Figure 5 shows the time that it takes for the SN shock to overtake this material, $t_{\rm flash}$. We estimate this time as $(R_* - R_{\rm br})/v_{\rm sh}$, where R_* is the radius of the model, $R_{\rm br}$ is the radial coordinate of the shock breakout, and $v_{\rm sh}$ is the shock velocity.

Figure 5 suggests that our models allow for up to few $10^{-2}\,M_\odot$ of material to be flash-ionized by the ultraviolet (UV) radiation from the shock breakout and emit narrow lines. These lines are expected to disappear within the time $t_{\rm flash}$, which constitutes few hours in our models. However, we emphasize that availability of mass above the shock breakout is not yet sufficient for the formation of flash-ionization lines (see, for example, Dessart et al. 2017). In addition, $t_{\rm flash}$ seen in our models is several times shorter than typical lifetime of observed flash-ionization lines. We anticipate that only simulations using more advanced radiation transport codes will be able to determine whether it is possible to explain the flash-ionization phenomenon seen in SNe II based on the outburst model suggested here.

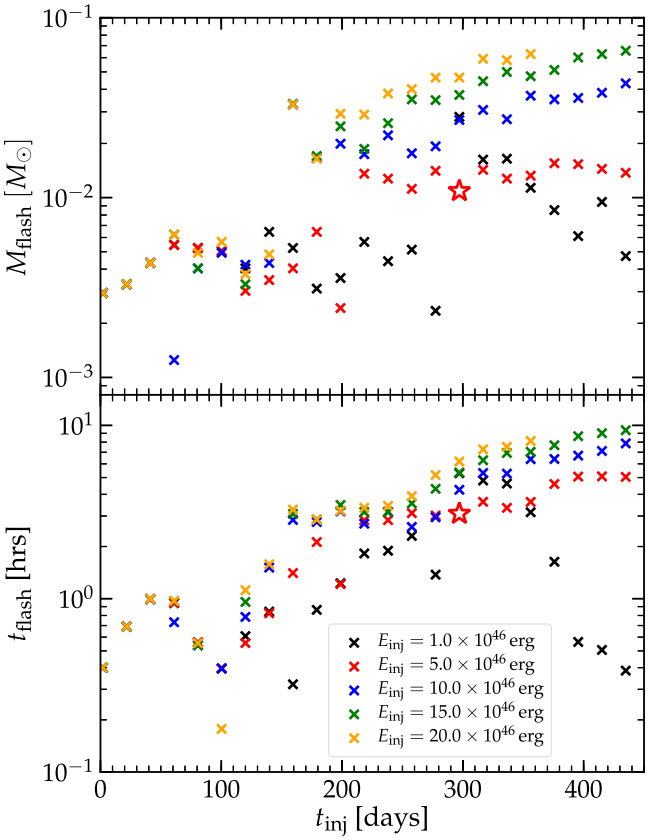

Figure 5. Top panel: the amount of mass that lays above the shock at the moment of breakout, as a function of $t_{\rm inj}$ for different energies $E_{\rm inj}$. Bottom panel: the time it takes for this material to be overtaken by the SN shock wave. The star marker in both panels corresponds to the best-fitting model from Figure 3.

4. Conclusions and Discussion

Our work demonstrates that even a moderate amount of energy (10^{46}–10^{47} erg) deposited into RSG envelopes during late-stage nuclear burning can dramatically impact the final SN IIP light curves. The envelope expansion and mass ejection caused by this energy deposition resembles the dense CSM that was used in previous works to explain the early luminosity excess in the observed SN IIP light curves compared to the bare RSG light curves (Morozova et al. 2017, 2018). The fact that such energy deposition is expected in RSGs due to wave energy transport from the core to the envelope (Fuller 2017) may explain the fact that the vast majority of SNe IIP benefit from the inclusion of some CSM in their light curve models (Das & Ray 2017; Förster et al. 2018; Moriya et al. 2018; Morozova et al. 2018; Paxton et al. 2018). In addition, the mass ejection caused by this energy deposition may explain the formation of the narrow, flash-ionization lines observed in the early spectra of many SNe II (Khazov et al. 2016). Therefore, it is important to follow late-stage nuclear burning in stellar evolution codes and ensure the proper energy exchange between the core and the envelope by means of the wave transport.

Recently Ouchi & Maeda (2019) investigated the influence of late-stage energy deposition on SN light curves by injecting a constant luminosity over a timescale of three years. When they use a high luminosity (super-Eddington), it is able to substantially change the structure of the RSG envelope, but Ouchi & Maeda (2019, p. 15) conclude that the "light curves and the evolution of photospheric velocity are all inconsistent with the observations of SNe II." For comparison, the duration of energy injection in our models varied in the range of 3–60 days (15 days for the best-fit model). The contrast between our work and the work of Ouchi & Maeda (2019) demonstrates that a more impulsive energy injection, as expected for late-stage nuclear burning in RSGs (Fuller 2017), is needed to provide better agreement with observations of SN 2017eaw (and likely other SNe II with similar light curves). At the same time, we note that any progenitor model whose density profile is similar to our best-fit model would also match the data. Wave-driven outbursts may not be required if wind acceleration (Moriya et al. 2018) or some other envelope heating mechanism is found to produce substantial CSM above the photosphere of stellar evolution models.

In addition to the rapid energy deposition during core Ne burning episode, the wave theory predicts steady envelope heating by a subsequent core O burning in the last months of RSG evolution (Figure 5 of Fuller 2017). While the rapid Ne burning leads to the CSM ejection from the surface of the RSG, the O burning was shown to inflate an evacuated bubble at the base of the H envelope, decrease the overall density of the envelope, and flatten its profile (Fuller 2017). This process is not taken into account in our models, and it indeed resembles more closely the setup studied by Ouchi & Maeda (2019; except for a shorter duration). We expect that this process would not influence the early light curves as much as it would change the slope of the plateau and its transition to the radioactive tail, perhaps contributing to the diversity of the observed Type II-P/II-L SN light curves. Further quantitative studies are required in order to fully understand the impact of the late-stage wave heating on the light curve and velocity evolution in Type II SNe.

Although our study does not provide quantitative predictions of the pre-SN outburst light curves, we can place constraints on their duration and amplitude. Our results suggest that the observable outburst should take place not earlier than a few years before the SN. This roughly agrees with the predictions of the wave heating model, in which wave heating during core Ne burning can produce an outburst months to years before core collapse (Fuller 2017). According to Figures 5 and 8 of Fuller (2017; cases $\eta = 1/3$ and $\eta = 1$), 2×10^{46} erg of energy deposited at the base of the RSG envelope would lead to ∼20% increase in the progenitor luminosity at the peak of the outburst, while the deposition of 6×10^{46} erg would lead to the peak luminosity increase of a factor of 2. The duration of the outburst is expected to be of the order of few months (see Figure 9 of Fuller 2017), after which both luminosity and effective temperature would approach their initial values. Our work also demonstrates that it can take considerable time (∼100 days or more) for the low-energy shock driven by wave heating to reach the stellar surface. This means that when observations of pre-explosion outbursts (or at least constraints on their occurrence) are made, this timescale for traversing the star should be taken into account when making comparisons to specific stages of nuclear burning.

The optical Large Binocular Telescope (LBT) archival images of SN 2017eaw were analyzed by Johnson et al. (2018), where no signs of the progenitor pre-explosion activity were found. Further analysis of the *Hubble Space Telescope* (*HST*) data by Rui et al. (2019) indicated a dimming of the progenitor by 30% one year before the explosion (see also Van Dyk et al. 2019). It is possible that the outburst could happen between the relatively scarce *HST* measurements. The temperature evolution in our simple models suggests that the ejected material may quickly become optically thin, while not forming too much dust to completely obscure the progenitor. In this view, it is important to calculate better multi-band predictions of the outburst light curves, which would provide a clearer picture of the outburst signatures that should be present in pre-explosion data. This will be especially helpful once the Vera C. Rubin Observatory (LSST Science Collaboration et al. 2009) is online, providing a long baseline of pre-explosion history for SN progenitors.

From Van Dyk et al. (2019), the progenitor of SN 2017eaw may have exhibited a moderate (∼40%) increase in the infrared *Spitzer* flux 1.6 yr before the explosion (although the measurement uncertainty is still too large to claim it to be a definite outburst). Another possibility is that an outburst occurred in the last ∼40 days before the SN explosion, where there is no *Spitzer* data. However, Keck and Palomar images taken days before the explosion do not show strong evidence for an outburst (Tinyanont et al. 2019), so we disfavor this possibility. Our current best model with $E_{\rm inj} = 5 \times 10^{46}$ erg (expected ∼50%–60% increase in the luminosity at the outburst peak) corresponds to the outburst happening ∼0.5 yr before the SN, which could not be captured by the available ground- and space-based observations. However, we emphasize that we have not carried out an extensive parameter survey, and it may be possible to find other stellar models (e.g., of different mass or radius) with different energy injection parameters that can fit both the pre-SN variability constraints and the SN light curve.

V.M. acknowledges helpful discussions with David Radice, James Stone, and Adam Burrows. A.L.P. acknowledges

financial support for this research from a Scialog award made by the Research Corporation for Science Advancement. This research is funded in part by a Rose Hills Innovator Grant, and by grant HST-AR-15021.001-A. Numerical simulations were performed using Della cluster of Princeton University, as well as computing services of the Institute for Computational and Data Sciences of the Pennsylvania State University.

ORCID iDs

Anthony L. Piro https://orcid.org/0000-0001-6806-0673
Jim Fuller https://orcid.org/0000-0002-4544-0750
Schuyler D. Van Dyk https://orcid.org/0000-0001-9038-9950

References

Buta, R. J., & Keel, W. C. 2019, MNRAS, 487, 832
Das, S., & Ray, A. 2017, ApJ, 851, 138
Dessart, L., John Hillier, D., & Audit, E. 2017, A&A, 605, A83
Förster, F., Moriya, T. J., Maureira, J. C., et al. 2018, NatAs, 2, 808
Fuller, J. 2017, MNRAS, 470, 1642
Gal-Yam, A., Arcavi, I., Ofek, E. O., et al. 2014, Natur, 509, 471
Georgy, C., Ekström, S., Granada, A., et al. 2013, A&A, 553, A24
Johnson, S. A., Kochanek, C. S., & Adams, S. M. 2018, MNRAS, 480, 1696
Khazov, D., Yaron, O., Gal-Yam, A., et al. 2016, ApJ, 818, 3
Kochanek, C. S. 2019, MNRAS, 483, 3762
Kochanek, C. S., Fraser, M., Adams, S. M., et al. 2017, MNRAS, 467, 3347
LSST Science Collaboration, Abell, P. A., Allison, J., et al. 2009, arXiv:0912.0201
Moriya, T. J., Förster, F., Yoon, S.-C., Gräfener, G., & Blinnikov, S. I. 2018, MNRAS, 476, 2840
Moriya, T. J., Yoon, S.-C., Gräfener, G., & Blinnikov, S. I. 2017, MNRAS, 469, L108
Morozova, V., Piro, A. L., Renzo, M., et al. 2015, ApJ, 814, 63
Morozova, V., Piro, A. L., & Valenti, S. 2017, ApJ, 838, 28
Morozova, V., Piro, A. L., & Valenti, S. 2018, ApJ, 858, 15
Morozova, V., & Stone, J. M. 2018, ApJ, 867, 4
Ofek, E. O., Sullivan, M., Cenko, S. B., et al. 2013, Natur, 494, 65
Ofek, E. O., Sullivan, M., Shaviv, N. J., et al. 2014, ApJ, 789, 104
O'Neill, D., Kotak, R., Fraser, M., et al. 2019, A&A, 622, L1
Ouchi, R., & Maeda, K. 2019, ApJ, 877, 92
Paxton, B., Schwab, J., Bauer, E. B., et al. 2018, ApJS, 234, 34
Quataert, E., Fernández, R., Kasen, D., Klion, H., & Paxton, B. 2016, MNRAS, 458, 1214
Quataert, E., & Shiode, J. 2012, MNRAS, 423, L92
Rui, L., Wang, X., Mo, J., et al. 2019, MNRAS, 485, 1990
Shiode, J. H., & Quataert, E. 2014, ApJ, 780, 96
Smartt, S. J. 2009, ARA&A, 47, 63
Sukhbold, T., Ertl, T., Woosley, S. E., Brown, J. M., & Janka, H.-T. 2016, ApJ, 821, 38
Tinyanont, S., Kasliwal, M. M., Krafton, K., et al. 2019, ApJ, 873, 127
Van Dyk, S. D. 2017, in Handbook of Supernovae, ed. A. W. Alsabti & P. Murdin (Cham: Springer), 693
Van Dyk, S. D., Zheng, W., Maund, J. R., et al. 2019, ApJ, 875, 136
Yaron, O., Perley, D. A., Gal-Yam, A., et al. 2017, NatPh, 13, 510